Article

An Electronic Skin Readout System for Liquid Metal based Flexible Resistive Sensor Array

Huan Qian ZHANG [1,ξ] Jee Chin TEOH [1, ξ] Jian-Feng Wu [2], Long Teng Yu [1,4], Rui-Heng Wang [2], Deleon Mark Francis [3], Chwee Teck Lim [1*]

[1.]National University of Singapore

henry.zhang@nus.edu.sg(HQ.Z); jcteoh@nus.edu.sg(JC.T); yu.longteng@u.nus.edu(LT.Y)

[2.]Southeast University

wjf@seu.edu.cn(JF.W); 220193353@seu.edu.cn(RH.W)

[3.]FlexoSense Pte Ltd

mark@flexosense.com(DM.F)

[4.]Microtube Technologies Pte Ltd

[*]Correspondence: ctlim@nus.edu.sg; Tel.:+65 65167801

Author Contributions: Huan Qian ZHANG and Jee Chin TEOH contributed equally.

Abstract - Liquid metal alloy, incorporated with microfluidic manipulation, has become a promising candidate for flexible resistive sensor array (RSA) that can imitate the functions of human skin. One advantage of RSA with shared rows and shared columns is to reduce the number of wires from M × N to M + N (rows: M and columns: N) and hence to greatly lessen the complexity and burden on the electrical system. The associated drawback is the crosstalk effect between adjacent elements during measurement. Although many literatures have reported several methods to resolve this limitation, almost all of them focus only on the high resistance value (≥100 Ω) RSA. There is a lack of detailed experimental data that addresses low resistance RSA with sensing elements below 100 Ω. Here, we aim to fill the gap of this field. We established two common RSA readout systems, i.e. zero potential methods (ZPM) (setting non-scanned-sampling-electrode zero potential (S-NSSE-ZP) and setting non-scanned-sampling-electrode zero potential with amplifier (S-NSSE-ZP-A)) and to compare their performances in low resistance value (≤100 Ω) RSA. For ideal resistor RSA, the measurement results show that S-NSSE-ZP has at least one time higher error than S-NSSE-ZP-A.

Keywords – Resistive sensor array, measurement error, zero potential methods, liquid metal, flexible electrical skin.

---

1. Introduction

Electronic skin (e-Skin) is a synthetic human skin, capable of detecting mechanical pressures of various intensities and frequencies. This emerging technology are now widely applied in medical and healthcare products, such as prosthesis, robotics, patient monitoring systems etc. [1]. On top of the demanding technical specification such as high sensitivity and quick responsiveness, e-Skin necessitates three key features that distinguishes it from other physical sensors, namely stretchability, flexibility and conformability. Soft elastomers come forth as an appealing substrate choice, based on the above-mentioned criteria.

Eutectic gallium indium (EGaIn), an alloy consisting of 75% gallium and 25% indium, is a low viscosity liquid metal at room temperature and has good electrical conductivity [2]. These unique characteristics of EGaIn accomplish the making of active components in soft sensors, which to measure strain and pressure [3-5] with varying capacitance and resistance values of EGaIn upon deformation.

Capacitive sensors have advantages of high spatial resolution and good frequency response. But they suffer from stray capacitance and field interaction when they are connected in a mesh network. Resistive sensors, on the other hand, are less susceptible to stray parameters and field interaction and hence they are favored in mesh network. One drawback of resistive sensors is lower frequency response as compared to capacitive sensors; nonetheless this limitation has negligible effect on e-Skin application as only low frequency forces come into play [6]. By encapsulating liquid metal with soft elastomers, our group has previously designed and fabricated single EGaIn based pressure sensors [7-9] with relatively low resistance range of 10 Ω baseline (no load), up to 20 Ω with car rolling and 200 Ω with foot stomping on it. The promising research outcome has successfully spin off two startup companies (i.e. FlexoSense Pte Ltd. and Microtube Technologies Pte Ltd.) specializing in sensing for healthcare and wearable electronics. Many of the key researches focus on alleviating the patient and healthcare system burden by realizing self-monitoring of health data, such as keeping track of foot plantar pressure in potential diabetic foot patients with the aid of flexible pressure sensing insole.

These sensors are soft, stretchable, conformable and sensitive to mechanical loading and have great potentials to be used as the building block of e-Skin. Without question, single sensor is not sufficient to duplicate the function of human skin which has densely packed mechanoreceptors with very small receptive fields. To achieve high spatial resolution, a large number of individual sensors have to be merged to form a resistive sensor array (RSA). RSA enables the increment of sensing element with minimal wire linkage and least possible burden to the electrical system. The only major concern is the crosstalk effects resulted from adjacent idle sensors that gives rise to additional measurement error.

A number of RSA readout systems have been proposed to eliminate the crosstalk effect. These approaches include inserting diode method (IDM)[10, 11], inserting transistor method (ITM) [12] [13-15], passive integrator method (PIM) [16-18], resistance matrix approach (RMA) [19], improved RMA [37] and incidence matrix approach (IMA) [20], voltage feedback method (VFM) [21-30] and zero potential method (ZPM) [29, 31-37]. Aforementioned systems only address high resistance designs; electronic networks with low resistance below 100 Ω are often left unattended. To date only one research [24] reported a mathematical simulation from 10 Ω to 100 kΩ; nonetheless, no detailed experimental data was presented in the range of 1 Ω to 100 Ω.

The low popularity and slow research progress on low resistance network is partially attributed to the technical challenges, such as larger crosstalk effect and associated greater PCB parasite effect that are adversely affecting the system performance. In addition, majority of the mechanical sensors and actuators in the market are high resistance transducers, due to the construction materials, fabrication techniques and sensing mechanisms involved.

Unquestionably, more effort is directed to study the more ubiquitous sensor array (>100 Ω) to improve usability.

More recently, however, there has been a growing interest in the development of liquid metal based RSA along with e-Skin, which registers low resistance value and inevitably triggers large PCB parasitic effect.

Here, we compared two commonly practiced readout system (setting non-scanned-sampling-electrode zero potential (S-NSSE-ZP) and setting non-scanned-sampling-electrode zero potential with amplifier (S-NSSE-ZP-A)) in order to decrease the crosstalk of the RSA system in PCB test. We first examined the effects in low value RSA and analyzed the electrical theory of these methods. We also demonstrated the best case analysis experiments with optimum circumstances.

2. Effects in low value RSA

One of the most notable effects in low value RSA is the crosstalk from adjacent unmeasured resistors.

As shown in Figure 1, the RSA is organized in the form 3*3 array. To calculate the resistance of the target resistor 'R_{22}', we require the current flowing through it and the voltage difference across the element which are denoted as 'I_{22}' and 'U_{22}' accordingly. 'U_{22}' equals the voltage difference between the row and column wire 'V_{row2} - V_{col2}'. However, current 'I_{22}' cannot be measured directly, as 'I_{col2}' on the column wire is not equivalent to 'I_{22}'. The crosstalk currents from unmeasured resistors will be measured as well. The dashed arrow line in Figure 1 illustrates one example of the crosstalk currents. Consequently, the actual value of 'R_{22}' cannot be calculated easily from '*Icol2*' and 'U_{22}'.

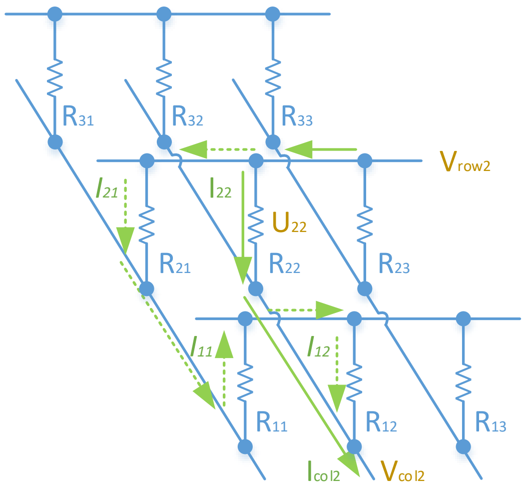

Figure 1. Crosstalk current of resistor array

Another drawback in low value RSA is the parasitic resistance originating from the conducting strands in the printed circuit board (PCB). A copper line with 0.254 mm width, 10 mm length and 1 oz thickness will have a resistance of 19 mΩ. It appears to be a fairly insignificant value, but it will actually contribute 1% error for a 2 Ω sensor. What should be noted is that each sensor has two end lines and crosstalk effect will magnify this parasitic effect. Totally error is further boosted by increasing the array size. Fortunately, this effect can be eliminated by using wider and thicker wires.

3. Readout circuit methods for RSA

Several methods, ZPM, VFM and IDM, have been developed to omit crosstalk effect. Based on a detailed comparative analysis [24], Liu concluded that ZPM has the best performance , as compared to VFM and IDM.

In this study, two types of ZPM are discussed, namely S-NSSE-ZP and S-NSSE-ZP-A, as shown in Figure 2. The difference between these two ZPM designs is that S-NSSE-ZP uses only one driving amplifier to run all the all rows and columns, while S-NSSE-ZP-A has one driving amplifier in each row and column. The tradeoff between circuit complexity and system performance is assessed carefully.

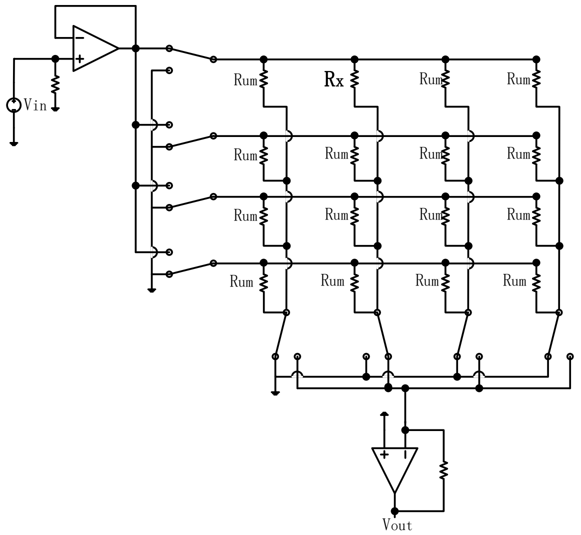

(a) S-NSSE-ZP method

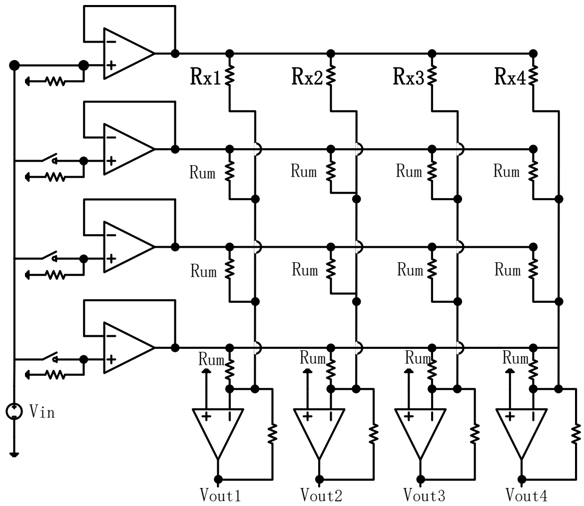

(b) S-NSSE-ZP-A method

Figure 2. (a) Circuit based on the S-NSSE-ZP method (b) Circuit based on the S-NSSE-ZP-A method

For S-NSSE-ZP method, resistor R_x is linked with two switches on each of its node. Two amplifiers drive resistor R_x through two switches. One amplifier provides driving voltage V_{in} on one node while the second amplifier clamps the second node to ground potential. V_{out} is generated by the second amplifier. The other unmeasured resistors R_{um}

are grounded through corresponding switches. The ideal measurement value can be calculated from Equation 1:

$$R_x = \frac{V_{in}}{I_f} = -\frac{V_{in}}{V_{out}} \times R_f \tag{1}$$

For S-NSSE-ZP-A method, resistor R_{xi} is linked with two amplifiers on each of its node. Resistor R_{xi} is driven by V_{in} and grounded by two amplifiers. V_{outi} is generated by the amplifier which forces one node of R_{xi} to ground. The other unmeasured resistors R_{um} are grounded through connected amplifiers. The ideal measurement value can be calculated from Equation 1 as well.

In the case of actual hardware system, two parasitic effects need to be included into the ideal equation, the switch ON resistor R_{ON} and amplifier offset voltage V_{OS}, as shown in Figure 2.

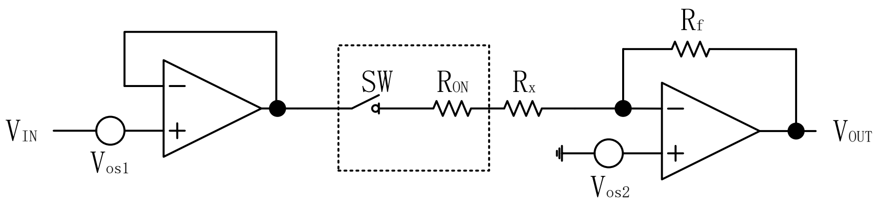

(a) S-NSSE-ZP method with parasitic effects

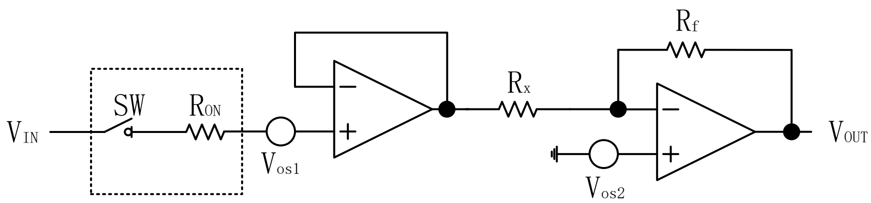

(b) S-NSSE-ZP-A method with parasitic effects

Figure 2. Circuit designs that include parasitic effects in the cases of (a) S-NSSE-ZP and (b) S-NSSE-ZP-A methods

Consequently, the actual measured resistance in Equation 1 has to be modified and the equations are depicted in Equation 2:

$$R_x = -\left(\frac{V_{in} - V_{OS1} - V_{OS2}}{V_{out}} \times R_f + R_{ON}\right) \tag{2-1}$$

$$R_x = -\left(\frac{V_{in} - V_{OS1} - V_{OS2}}{V_{out}} \times R_f\right) \tag{2-2}$$

The major difference between the above mentioned two methods is that S-NSSE-ZP-A method is capable of eliminating the parasitic effect of R_{ON} with the use of amplifiers in each row and column, whereas S-NSSE-ZP does not. However, Figure 2 is just a simplified model without crosstalk effect, which is different from the more practical applications and scenarios such as sensors array in e-Skin, whereby crosstalk is not negligible (Figure 3).

Figure 3 shows an example of 2*2 RSA with the crosstalk effect. In order to include parasitic effect of R_{ON} in this model, we use S-NSSE-ZP method for analyzing.

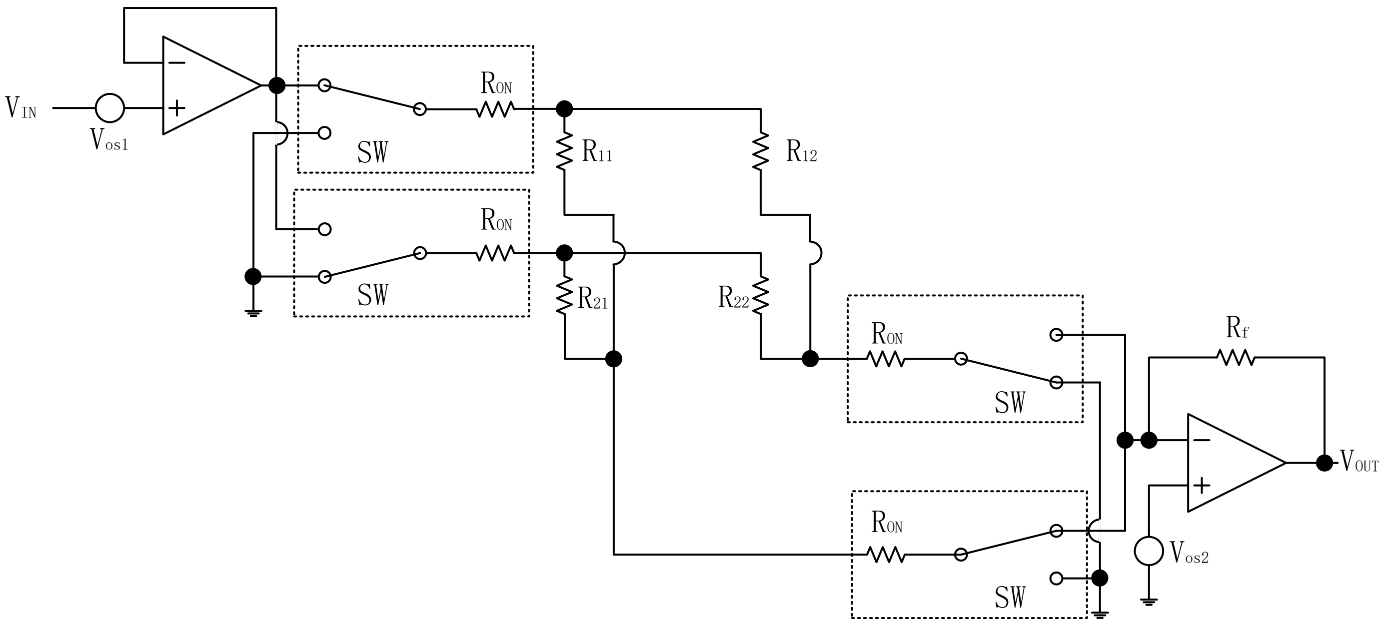

Figure 3. 2×2 array circuit model including parasitic effects and crosstalk effect for S-NSSE-ZP method

In order to calculate the existing crosstalk effect, we extract the array network and apply Kirchhoff Laws to analyze the network, as shown in Figure 4 and Equation 3.

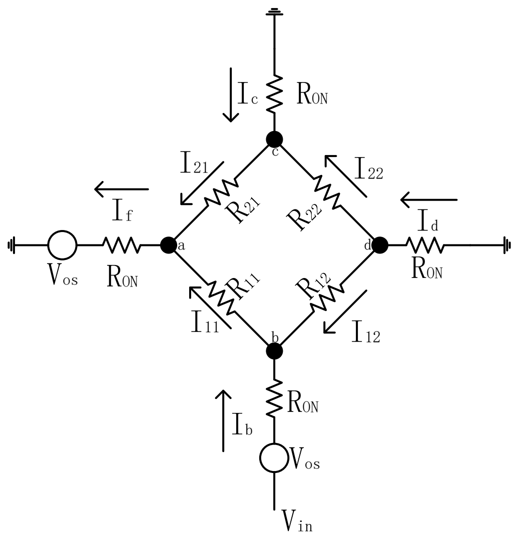

Figure 4. Array network extracted and analyzed with Kirchhoff law

$$V_a = V_{os} + I_f \cdot R_{ON} = V_{os} + (I_{21} + I_{11}) \cdot R_{ON} \qquad (3-1)$$

$$V_b = V_{os} + V_{in} - I_b \cdot R_{ON} = V_{os} + V_{in} - (I_{12} + I_{11}) \cdot R_{ON} \qquad (3-2)$$

$$V_c = -I_c \cdot R_{ON} = -(I_{21} + I_{22}) \cdot R_{ON} \qquad (3-3)$$

$$V_d = -I_d \cdot R_{ON} = (I_{12} + I_{22}) \cdot R_{ON} \qquad (3-4)$$

$$V_b - V_a = I_{11} \cdot R_{11} \qquad (3-5)$$

$$V_c - V_a = I_{21} \cdot R_{21} \qquad (3-6)$$

$$V_b - V_d = I_{12} \cdot R_{12} \qquad (3-7)$$

$$V_c - V_d = I_{22} \cdot R_{22} \qquad (3-8)$$

We hypothesize that $R_{11} = R_x$ and $R_{12} = R_{21} = R_{22} = R$ and $10 \cdot R_{ON} < R \approx R_x$. After substituting (3-1, 3-2, 3-3, 3-4) to (3-5, 3-6, 3-7, 3-8), we obtain Equation 4.

$$I_{11}(R_x + 2R_{ON}) + I_{12}R_{ON} + I_{21}R_{ON} + I_{22} \cdot 0 = V_{in} \qquad (4-1)$$

$$I_{11}R_{ON} + I_{12} \cdot 0 + I_{21}(R + 2R_{ON}) + I_{22}R_{ON} = -V_{os} \qquad (4-2)$$

$$I_{11}R_{ON} + I_{12}(R + 2R_{ON}) + I_{21} \cdot 0 + I_{22}R_{ON} = V_{os} + V_{in} \qquad (4-3)$$

$$I_{11} \cdot 0 + I_{12}R_{ON} + I_{21}R_{ON} + I_{22}(R + 2R_{ON}) = 0 \qquad (4-4)$$

Equation 4 is a nonhomogeneous linear equation $R \cdot I = V$ and it can be written as Equation 5.

$$\left(\begin{array}{cccc|c} R_x + 2R_{ON} & R_{ON} & R_{ON} & 0 & V_{in} \\ R_{ON} & 0 & R + 2R_{ON} & R_{ON} & -V_{os} \\ R_{ON} & R + 2R_{ON} & 0 & R_{ON} & V_{os} + V_{in} \\ 0 & R_{ON} & R_{ON} & R + 2R_{ON} & 0 \end{array}\right) \tag{5}$$

We define $R + 2R_{ON} = R_+$ and $R_x + 2R_{ON} = R_{x+}$, then we have:

$$\left(\begin{array}{cccc|c} R_{x+} & R_{ON} & R_{ON} & 0 & V_{in} \\ R_{ON} & 0 & R_+ & R_{ON} & -V_{os} \\ R_{ON} & R_+ & 0 & R_{ON} & V_{os} + V_{in} \\ 0 & R_{ON} & R_{ON} & R_+ & 0 \end{array}\right) \tag{6}$$

After rearranging, we have:

$$\left(\begin{array}{cccc|c} 1 & 0 & 0 & -R_+/R_{x+} & V_{in}/R_{x+} \\ 1 & 0 & R_+/R_{ON} & 1 & -V_{os}/R_{ON} \\ 0 & 1 & -1 & 0 & (2V_{os} + V_{in})/R_+ \\ 0 & 1 & 1 & R_+/R_{ON} & 0 \end{array}\right) \tag{7}$$

Rearranging row 2 and 3, we have:

$$\left(\begin{array}{cccc|c} 1 & 0 & 0 & -R_+/R_{x+} & V_{in}/R_{x+} \\ 0 & 0 & R_+/R_{ON} & 1 + R_+/R_{x+} & -V_{os}/R_{ON} - V_{in}/R_{x+} \\ 0 & 0 & -2 & -R_+/R_{ON} & (2V_{os} + V_{in})/R_+ \\ 0 & 1 & 1 & R_+/R_{ON} & 0 \end{array}\right) \tag{8}$$

Rearranging row 3, we have:

$$\left(\begin{array}{cccc|c} 1 & 0 & 0 & -R_+/R_{x+} & V_{in}/R_{x+} \\ 0 & 0 & R_+/R_{ON} & 1 + R_+/R_{x+} & -V_{os}/R_{ON} - V_{in}/R_{x+} \\ 0 & 0 & 0 & 1 & -V_{in}R_{ON}R_x/2{R_+}^2R_{x+} \\ 0 & 1 & 1 & R_+/R_{ON} & 0 \end{array}\right) \tag{9}$$

Rearranging row 1, we have:

$$\left(\begin{array}{cccc|c} 1 & 0 & 0 & 0 & V_{in}(2R_{x+}R_+ - R_{ON}R_x)/2{R_{x+}}^2R_+ \\ 0 & 0 & R_+/R_{ON} & 1 + R_+/R_{x+} & -V_{os}/R_{ON} - V_{in}/R_{x+} \\ 0 & 0 & 0 & 1 & -V_{in}R_{ON}R_x/2{R_+}^2R_{x+} \\ 0 & 1 & 1 & R_+/R_{ON} & 0 \end{array}\right) \tag{10}$$

Rearranging row 2, we have:

$$\left(\begin{array}{cccc|c} 1 & 0 & 0 & 0 & V_{in}(2R_{x+}R_+ - R_{ON}R_x)/2{R_{x+}}^2R_+ \\ 0 & 0 & 1 & 0 & -V_{os}/R_+ - V_{in}R_{ON}\left(2R_{x+}{R_+}^2 - R_xR_{ON}R_{x+} - R_xR_+R_{ON}\right)/2{R_{x+}}^2{R_+}^3 \\ 0 & 0 & 0 & 1 & -V_{in}R_{ON}R_x/2{R_+}^2R_{x+} \\ 0 & 1 & 1 & 0 & -V_{in}R_x/2R_+R_{x+} \end{array}\right) \tag{11}$$

Rearranging row 2, row 3 and row 4 again, we have:

$$\left(\begin{array}{cccc|c} 1 & 0 & 0 & 0 & V_{in}(2R_{x+}R_+ - R_{ON}R_x)/2{R_{x+}}^2R_+ \\ 0 & 1 & 0 & 0 & -V_{in}R_x/2R_+R_{x+} + V_{os}/R_+ + V_{in}R_{ON}\left(2R_{x+}{R_+}^2 - R_xR_{ON}R_{x+} - R_xR_+R_{ON}\right)/2{R_{x+}}^2{R_+}^3 \\ 0 & 0 & 1 & 0 & -V_{os}/R_+ - V_{in}R_{ON}\left(2R_{x+}{R_+}^2 - R_xR_{ON}R_{x+} - R_xR_+R_{ON}\right)/2{R_{x+}}^2{R_+}^3 \\ 0 & 0 & 0 & 1 & -V_{in}R_{ON}R_x/2{R_+}^2R_{x+} \end{array}\right) \tag{12}$$

From (3-1), we have $I_f = I_{21} + I_{11}$. From (12) row 1 (I_{11}) and 3 (I_{21}), we have:

$$I_f = -V_{os}/R_+ - V_{in}R_{ON}\left(2R_{x+}{R_+}^2 - R_xR_{ON}R_{x+} - R_xR_+R_{ON}\right)/2{R_{x+}}^2{R_+}^3 + V_{in}(2R_{x+}R_+ - R_{ON}R_x)/2{R_{x+}}^2R_+ \tag{13}$$

After simplifying, we have:

$$I_f = \frac{-3R_{ON}R_x + 2R_xR + 4(R + R_x)R_{ON}}{2{R_x}^2R + 4R_{ON}\left({R_x}^2 + 2RR_x\right)}V_{in} - \frac{V_{os}}{R + 2R_{ON}} \tag{14}$$

We can evaluate I_f from Equation (14) by assuming R_{ON} and V_{os} equal to zero (ideal case), then $I_f = \frac{V_{in}}{R_x}$ and it matches equation (1).

Even though Equation (14) is derived from S-NSSE-ZP method, it can also be applied in the case of S-NSSE-ZP-A given that $R_{ON} = 0$, as shown in Equation (15):

$$I_f = \frac{V_{in}}{R_x} - \frac{V_{os}}{R} \tag{15}$$

and it matches Equation (2-2).

From Equation (1), we know for S-NSSE-ZP method:

$$V_{out} = -I_f \times R_f = -\frac{-3R_{ON}R_x + 2R_xR + 4(R+R_x)R_{ON}}{2{R_x}^2R + 4R_{ON}\left({R_x}^2 + 2RR_x\right)}V_{in}R_f + \frac{V_{os}R_f}{R + 2R_{ON}} \tag{16}$$

And we know for S-NSSE-ZP-A method:

$$V_{out} = -I_f \times R_f = -\frac{-3R_{ON}R_x + 2R_xR + 4(R+R_x)R_{ON}}{2{R_x}^2R + 4R_{ON}\left({R_x}^2 + 2RR_x\right)}V_{in}R_f + \frac{V_{os}R_f}{R + 2R_{ON}} - \frac{V_{os}R_f}{R} \tag{17}$$

4. Best-case Circuit Analysis

In this section, best-case circuits are examined. Various experiments have been designed to evaluate the performances of the S-NSSE-ZP method and the S-NSSE-ZP-A method under optimum circumstances, with varying parameters such as switch resistor value (R_{ON}), array size (S_{AR}), unmeasured array resistors value (R_{um}) and measured resistor value (R_x).

The output amplifier's voltage of an ideal single resistor is represented as V_{id}. Meanwhile, the output amplifier's voltage of array resistors is measured as V_{arr}. The measurement error between them are evaluated as follows:

$$e\% = \frac{V_{id} - V_{arr}}{V_{id}} \times 100 \tag{18}$$

The number of possible outcomes, from the combination of the selected 4 varying parameters, is too large to be studied. Many of these combinations are less useful and lack practical application. To optimize the experiment effort and outcome, only sets of experiments (EXP) with carefully chosen combinations are analyzed (Table 1). The switches resistances (R_{ON}) of S-NSSE-ZP have several value such as: 0.5Ω, 1 Ω, 1.5 Ω, 2 Ω, 2.5 Ω, 3 Ω, 3.5 Ω, 50 Ω and 53.5 Ω. The array size (S_{AR}) is in the range of 2×2, 3×3, 4×4, 5×5, 6×6, 7×7 and 8×8. The unmeasured array resistors values (R_{um}) are 1 Ω, 5 Ω, 10 Ω, 50 Ω, 100 Ω and 200 Ω. The measured resistor values (R_x) are: 1 Ω to 10 Ω with 1 Ω each step, 19 Ω to 20 Ω with 1 Ω each step, 20 Ω to 100 Ω with 10 Ω each step, 100 Ω to 200 Ω with 10 Ω each step.

Table 1. Experiments with selected combinations

EXP 1				EXP 2				EXP 3			
R_x(Ω)	R_{um}(Ω)	S_{AR}	R_{ON}(Ω)	R_x(Ω)	R_{um}(Ω)	S_{AR}	R_{ON}(Ω)	R_x(Ω)	R_{um}(Ω)	S_{AR}	R_{ON}(Ω)
All	1	2×2	0	All	1	2×2	0	1		2×2	0
values	200	3×3		values	5			200			0.5
		4×4			10						1
		5×5			50						1.5
		6×6			100						2
		7×7			200						2.5
		8×8									3
											3.5
											50
											53.5

EXP 1 analyzed the effect of array size S_{AR} on $e\%$ with the best state of switch resistor R_{ON} and the worst/best states of unmeasured array resistors R_{um}.

EXP 2 analyzed the effect of unmeasured array resistors R_{um} on $e\%$ with the best state of switch resistor R_{ON} and the best state of array size S_{AR}.

EXP 3 analyzed the effect of different switch resistor value R_{ON} on $e\%$ with the best state of array size S_{AR} and the worst/best state of unmeasured array resistors R_{um} and measured resistor R_x.

The best and the worst states refer the minimum and the maximum $e\%$ in (16) and (17).

The two parallel connected amplifiers used in S-NSSE-ZP method are OPA197, because of its low V_{os} (100uV) and relatively high output current (65mA). High output current is important for S-NSSE-ZP circuit design, as the whole array is driven by only one amplifier. It is difficult to find one single suitable amplifier that owns these two characteristics, as high drive ability and low V_{os} are opposite in nature and cannot be satisfied simultaneously. In order to increase the driving ability without raising V_{os}, we used two parallel connected amplifiers. The switches used in S-NSSE-ZP method are TS3A24159, because of its low ON state resistance (0.3 Ω).

Meanwhile in S-NSSE-ZP-A design, the amplifiers used are OPA4388, because of their low V_{os} (2.25μV). The switches are ADG804, due to the low ON state resistor (0.5 Ω). However, it is not a critical parameter for this method.

Because of the power supply requirement of OPA197 and OPA4388, S-NSSE-ZP and S-NSSE-ZP-A are supplied with 3.3V and 2.5V power sources respectively.

The experimental setup is shown in Figure 5. We can change R_{sw} of S-NSSE-ZP by plugging in/out the wiring cap of the experimental resistors. Different S_{AR} and R_{um} are realized by using PCB arrays with varying S_{AR} and R_{um} value. The value of R_x is adjusted by the resistor box. Figure 5 is the hardware experimental system.

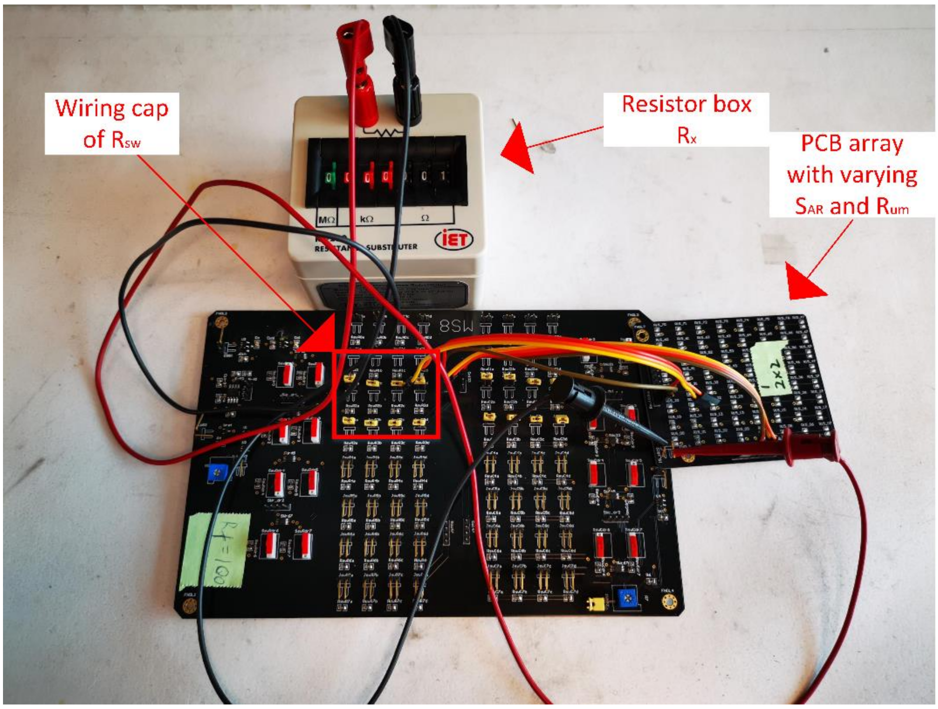

Figure 5. Experimental setup for S-NSSE-ZP and S-NSSE-ZP-A design (only S-NSSE-ZP is shown)

5. Results and Discussion

S-NSSE-ZP method is labeled as 8sw in the result graphs, as 1 amplifier and 8 switches are used to drive the array resistors arranged in rows or columns. S-NSSE-ZP-A method is named as 8op, as 8 amplifiers are adopted.

Figure 6 shows the error in S-NSSE-ZP and S-NSSE-ZP-A method when R_{um} is 200 Ω and S_{AR} changes from 1*1 to 8*8.

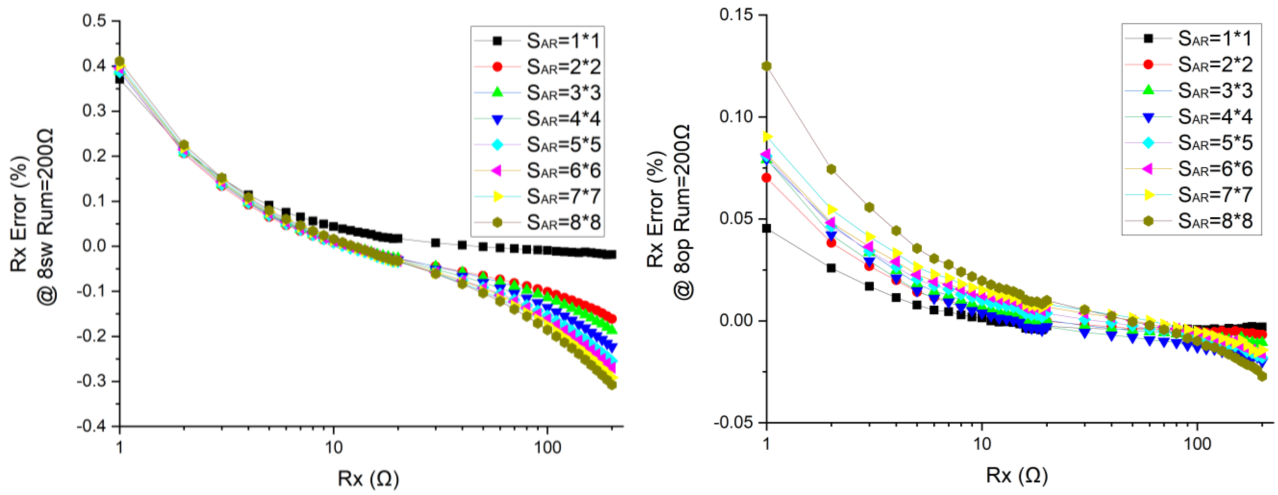

Figure 6. The effect of R_x on measurement error of different S_{AR} when $R_{um} = 200\Omega$ in S-NSSE-ZP and S-NSSE-ZP-A method.

Figure 7 shows the error in S-NSSE-ZP and S-NSSE-ZP-A method when R_{um} is 1 Ω and S_{AR} changes from 1×1 to 8×8.

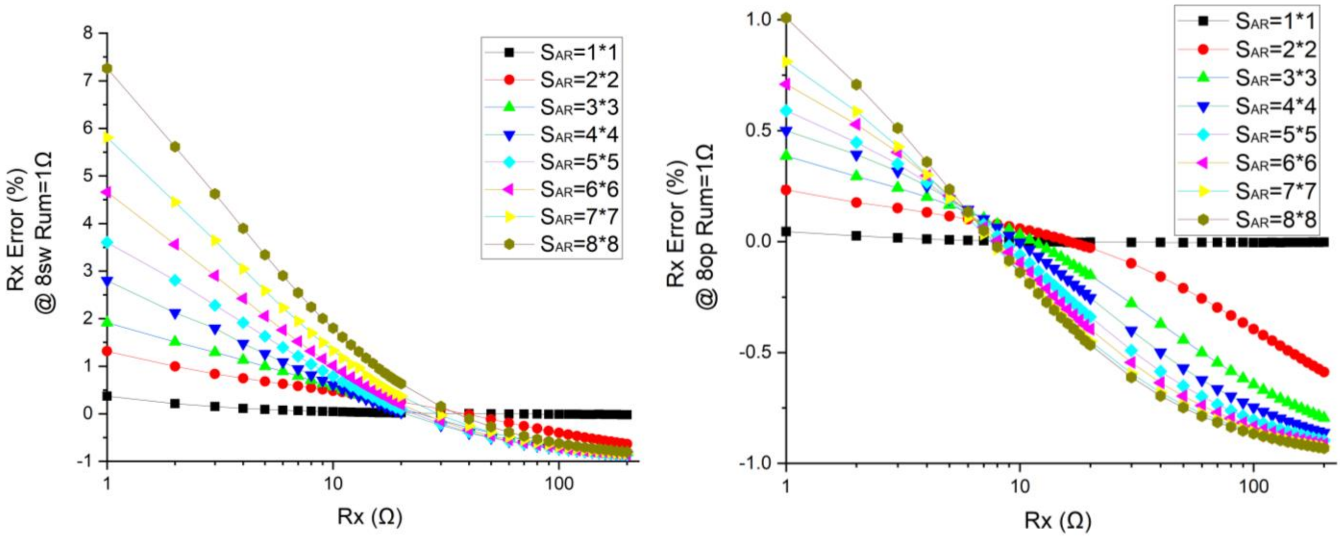

Figure 7. The effect of R_x on measurement error of different S_{AR} when $R_{um} = 1\Omega$ in S-NSSE-ZP and S-NSSE-ZP-A method.

Figure 8 shows the error in S-NSSE-ZP and S-NSSE-ZP-A method when $S_{AR} = 2 \times 2$ and R_{um} changes from 1 Ω to 200 Ω.

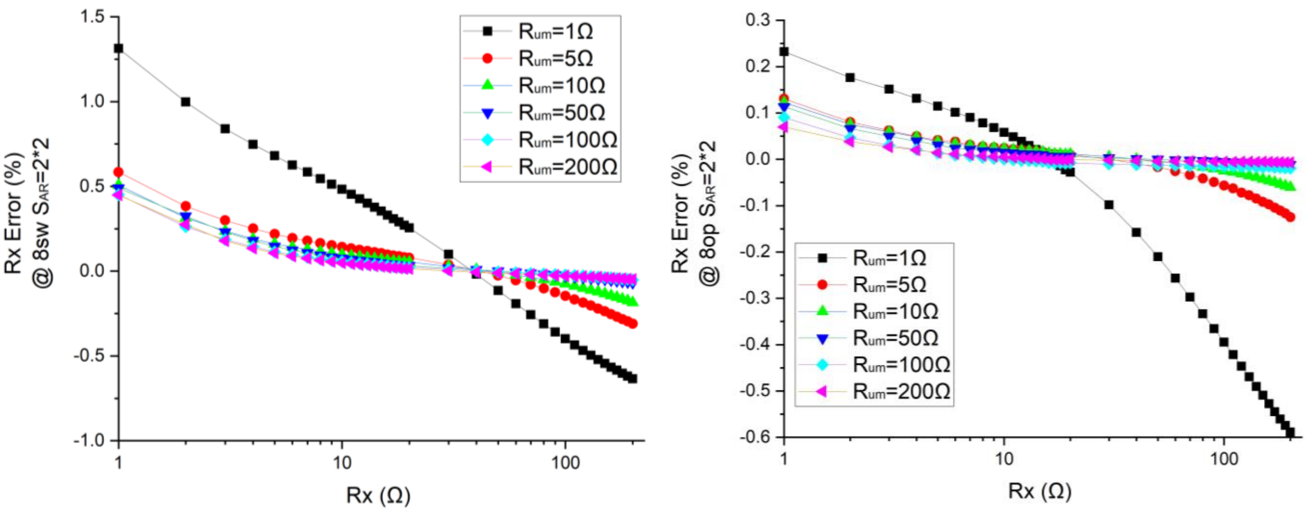

Figure 8. The effect of R_x on measurement error of different R_{um} when $S_{AR} = 2 \times 2$ in S-NSSE-ZP and S-NSSE-ZP-A method.

Figure 9 shows the error in S-NSSE-ZP method of different R_{sw} when $S_{AR} = 2 \times 2$.

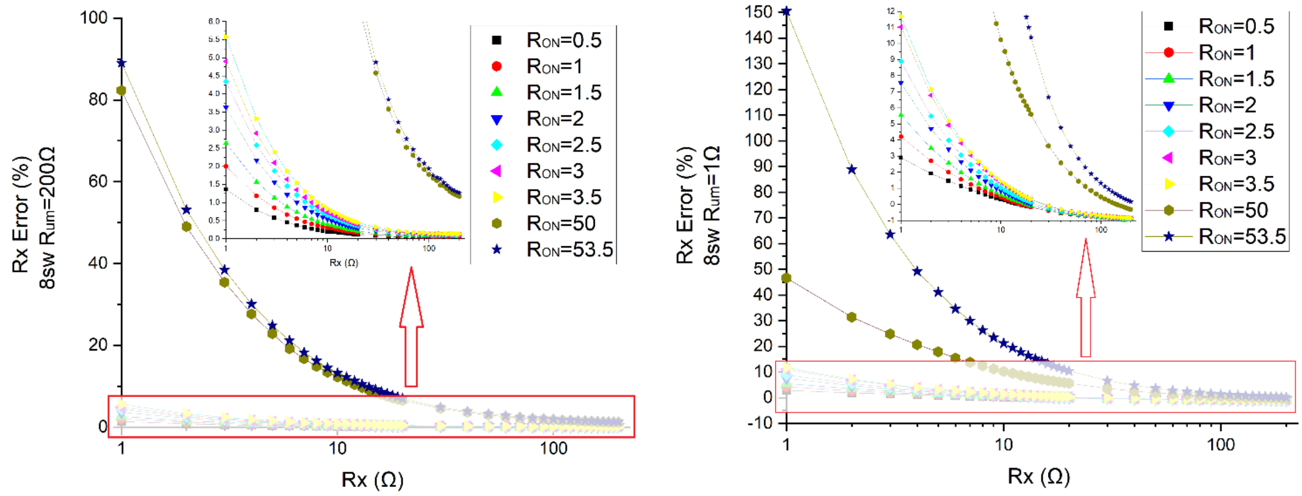

Figure 9. The effect of R_x on measurement error of different R_{sw} when $S_{AR} = 2 \times 2$.

As shown in Fig. 6, the error of 8sw is twice higher than 8op. That is because 8sw is restricted by R_{sw} and amplifier driving ability.

In Fig. 6, when the R_x is increasing from 1Ω to 100Ω, both errors of 8sw and 8op will decrease quickly. This is because the effect of connect wire parasitic resistor and PCB trace resistor will decrease with increasing R_x.

Also, when R_x is larger than 100 Ω, the error will increase again. We think it is the result of the real hardware limitation. As shown in Fig. 2, the output amplifier has a feedback resistor which is 100 Ω in our design. If the R_x is more than 100 Ω, the gain of amplifier will be less than 1. As the $V_{in} = 10\,mV$, so the V_{out} will be less than 10mV. We can rewrite equation (2-1) as equation (18). When V_{out} is decreasing, the middle term in the right side of equation (18) will increase and the error effect of V_{OS1} and V_{OS2} will also increase. So the totally error will increase.

$$R_x = -\left(\frac{V_{in}}{V_{out}} \times R_f - \frac{V_{OS1}+V_{OS2}}{V_{out}} \times R_f + R_{ON}\right) \quad (18)$$

A more common way to explain this phenomenon is that V_{out} is limited in a small range when gain is less than 1. The effect of V_{OS} will increase with decreasing V_{out}.

In Fig. 6, the array size change leads to a monotonic change in error.

As shown in Fig. 7, the error of 8sw and 8op is much higher than in Fig. 6. This is because R_{um} changed from 200 Ω in Fig. 6 to 1 Ω in Fig. 7. The smaller R_{um} needs the larger driving ability, which is limited by the amplifier feature. In Fig. 7, we can see the errors converge to a negative value instead of zero. That is because the simple equation (2) cannot match the real system when R_{um} decreases to 1 Ω. The crosstalk effect is the dominant error now. We should use equations (16) and (17) which are derived from crosstalk effect to analyze this phenomenon. The last term in the right side of equation (16) and (17) is a constant, so that it will form an offset after the first item converge to its minimum.

In Fig. 7, the array size change leads to a monotonic change in error.

In Fig. 8, we can see the error of 8sw is higher than 8op. This is because 8op has 8 separated amplifiers and each one of them has enough driving ability to force one column or row resistors, but 8sw has only one amplifier and its driving ability is not enough for the whole array of resistors.

We can see the error converge to an offset value when R_x increases as well. With increasing R_{um}, the offset value will decrease. This can be proven by the last term in the right side of equation (17) and (18) as well.

In Fig. 9, we can see the error of 8sw increases with R_{sw}. There is a negative convergent offset when $R_{um} = 1$ and zero convergent offset when $R_{um} = 200$. Both can be proven by equations (16) and (17). As the last term in equation (16) and (17) is divided by R which is rewritten as R_{um} here, thus the larger R_{um} leads to the smaller offset.

From the above analysis, we can make some suggestions in the design of an actual hardware system to measure low value RSA.

- Decreasing the connection wire, PCB trace and switch resistor.
- Increasing the amplifiers current driving ability.

- Decreasing the offset voltage of all amplifiers and making sure their offset voltage is equalized to zero.
- Decreasing the array size and separating large array to several independent small arrays.
- As the power cost increases greatly with array size, it is not recommended to use this circuit design in battery driven wearable system, especially without any low power design.
- S-NSSE-ZP-A method has lower error than S-NSSE-ZP method, because this method bypasses the switch resistor and has enough amplifier current driving ability.

6. Conclusions

We discussed the designs of S-NSSE-ZP and S-NSSE-ZP-A methods and established their simplified models and derived their output voltage equations. We also analyzed their measurement error with different array size, unmeasured resistor value, switch resistor value and measured resistor value. Several design suggestions are made for low value RSA measurement system. The results revealed S-NSSE-ZP-A has smaller resistor measurement error than S-NSSE-ZP.

References

1. Chortos, A., J. Liu, and Z. Bao, Pursuing prosthetic electronic skin. *Nature materials*, **2016**. *15*(9): p. 937.
2. Dickey, M.D., Stretchable and soft electronics using liquid metals. *Advanced Materials*, **2017**. *29*(27): p. 1606425.
3. Cheng, S. and Z. Wu, A Microfluidic, Reversibly Stretchable, Large - Area Wireless Strain Sensor. *Advanced Functional Materials*, **2011**. *21*(12): p. 2282-2290.
4. Roberts, P., et al. Soft-matter capacitive sensor for measuring shear and pressure deformation. in *2013 IEEE International Conference on Robotics and Automation*. **2013**. IEEE.
5. Vogt, D.M., Y.-L. Park, and R.J. Wood, Design and characterization of a soft multi-axis force sensor using embedded microfluidic channels. *IEEE sensors Journal*, **2013**. *13*(10): p. 4056-4064.
6. Tiwana, M.I., S.J. Redmond, and N.H. Lovell, A review of tactile sensing technologies with applications in biomedical engineering. *Sensors and Actuators A: physical*, **2012**. *179*: p. 17-31.
7. Yeo, J.C., et al., Wearable tactile sensor based on flexible microfluidics. *Lab on a chip*, **2016**. *16*(17): p. 3244-3250.
8. Yeo, J.C., et al., Triple-state liquid-based microfluidic tactile sensor with high flexibility, durability, and sensitivity. *Acs Sensors*, **2016**. *1*(5): p. 543-551.
9. Yu, L., et al., Highly stretchable, weavable, and washable piezoresistive microfiber sensors. *ACS applied materials & interfaces*, **2018**. *10*(15): p. 12773-12780.
10. Snyder, W.E. and J.S. Clair, Conductive elastomers as sensor for industrial parts handling equipment. *J IEEE Transactions on Instrumentation*

Measurement, **1978**. *27*(1): p. 94-99.

11. Prutchi, D. and M. Arcan, Dynamic contact stress analysis using a compliant sensor array. *Measurement*, **1993**. *11*(3): p. 197-210.
12. Tanaka, A., et al., Infrared focal plane array incorporating silicon IC process compatible bolometer. *IEEE transactions on Electron Devices*, **1996**. *43*(11): p. 1844-1850.
13. Takei, K., et al., Nanowire active-matrix circuitry for low-voltage macroscale artificial skin. *Nature materials*, **2010**. *9*(10): p. 821.
14. Wang, C., et al., User-interactive electronic skin for instantaneous pressure visualization. *Nature materials*, **2013**. *12*(10): p. 899.
15. Kane, B.J., M.R. Cutkosky, and G.T. Kovacs, A traction stress sensor array for use in high-resolution robotic tactile imaging. *Journal of microelectromechanical systems*, **2000**. *9*(4): p. 425-434.
16. Vidal-Verdú, F., et al., Three realizations and comparison of hardware for piezoresistive tactile sensors. *Sensors*, **2011**. *11*(3): p. 3249-3266.
17. Oballe-Peinado, Ó., et al., Accuracy and resolution analysis of a direct resistive sensor array to FPGA interface. *Sensors*, **2016**. *16*(2): p. 181.
18. Oballe-Peinado, Ó., et al., Improved circuits with capacitive feedback for readout resistive sensor arrays. *Sensors*, **2016**. *16*(2): p. 149.
19. Shu, L., X. Tao, and D.D. Feng, A new approach for readout of resistive sensor arrays for wearable electronic applications. *IEEE Sensors Journal*, **2014**. *15*(1): p. 442-452.
20. Lorussi, F., et al., Wearable, redundant fabric-based sensor arrays for reconstruction of body segment posture. *IEEE sensors Journal*, **2004**. *4*(6): p. 807-818.
21. Tise, B. A compact high resolution piezoresistive digital tactile sensor. in *Proceedings. 1988 IEEE International Conference on Robotics and Automation*. **1988**. IEEE.
22. Speeter, T.H. Flexible, piezoresitive touch sensing array. in *Optics, Illumination, and Image Sensing for Machine Vision III*. **1989**. International Society for Optics and Photonics.
23. Speeter, T.H., A tactile sensing system for robotic manipulation. *The International Journal of Robotics Research*, **1990**. *9*(6): p. 25-36.
24. Liu, H., et al., Measurement errors in the scanning of resistive sensor arrays. *Sensors Actuators A: Physical*, **2010**. *163*(1): p. 198-204.
25. D'Alessio, T., Measurement errors in the scanning of piezoresistive sensors arrays. *Sensors Actuators A: Physical*, **1999**. *72*(1): p. 71-76.

26. Wu, J., et al., A small size device using temperature sensor array. *Chin. J. Sens. Actuators*, **2011**. *24*(11): p. 1649-1652.
27. Wu, J., L. Wang, and J. Li, Design and crosstalk error analysis of the circuit for the 2-D networked resistive sensor array. *IEEE Sensors Journal*, **2014**. *15*(2): p. 1020-1026.
28. Wu, J., et al., A novel crosstalk suppression method of the 2-D networked resistive sensor array. *Sensors*, **2014**. *14*(7): p. 12816-12827.
29. Wu, J., et al., Cable crosstalk suppression with two-wire voltage feedback method for resistive sensor array. *Sensors*, **2016**. *16*(2): p. 253.
30. Wu, J., L. Wang, and J. Li, General voltage feedback circuit model in the two-dimensional networked resistive sensor array. *Journal of Sensors*, **2015**. *2015*.
31. Lazzarini, R., R. Magni, and P. Dario. A tactile array sensor layered in an artificial skin. in *Proceedings 1995 IEEE/RSJ International Conference on Intelligent Robots and Systems. Human Robot Interaction and Cooperative Robots*. **1995**. IEEE.
32. Saxena, R.S., et al., Virtual ground technique for crosstalk suppression in networked resistive sensors. *IEEE Sensors Journal*, **2010**. *11*(2): p. 432-433.
33. Yarahmadi, R., A. Safarpour, and R. Lotfi, An improved-accuracy approach for readout of large-array resistive sensors. *IEEE Sensors Journal*, **2015**. *16*(1): p. 210-215.
34. Wu, J. and L. Wang, Cable crosstalk suppression in resistive sensor array with 2-wire S-NSDE-EP method. *Journal of Sensors*, **2016**. *2016*.
35. Kim, J.-S., D.-Y. Kwon, and B.-D. Choi, High-accuracy, compact scanning method and circuit for resistive sensor arrays. *Sensors*, **2016**. *16*(2): p. 155.
36. Wu, J., et al., A novel two-wire fast readout approach for suppressing cable crosstalk in a tactile resistive sensor array. *Sensors*, **2016**. *16*(5): p. 720.
37. Wu, J. and J. Li, Approximate model of zero potential circuits for the 2-D networked resistive sensor array. *IEEE Sensors Journal*, **2016**. *16*(9): p. 3084-3090.